Analysis of the topography of a Bragg grating in chalcogenide glass

S.H. Messaddeq[a,*], M. Siu Li[a], U. Werner[b], Y. Messaddeq[c], D. Lezal[d], M.A. Aegerter[b]

[a]*Instituto de Física de São Carlos, USP, C.P. 369, CEP 13560-970, São Carlos, SP, Brazil*
[b]*Institut fur Neue Materialien, Im Stadtwald, Gebaude 43, D-66123 Sarrbrucken, Germany*
[c]*Instituto de Química, UNESP, C.P. 355, CEP 14801-970, Araraquara, SP, Brazil*
[d]*Laboratory of Inorganic Materials, IIC ASCR and ICT, Pelleova 24, Prague 6, Czech Republic*

Abstract

Relief Bragg gratings were recorded on the surface of Ga–Ge–S glass samples by interference of two UV laser beams at 351 nm. Scanning force microscopy was used to perform a 3D image analysis of the resulting surface topography, which shows the superposition of an imprinted grating over the base topography of the glass. An important question regarding the efficiency of the grating is to determine to what extent the base topography reduces the intended coherent scattering of the grating because of its stochastic character. To answer this question we separated both base and grating structures by Fourier filtering, examined both spatial frequency and roughness, and determined the correlation.

Keywords: Light-induced effects; Chalcogenide glasses; Atomic force microscopy; Relief gratings

1. Introduction

Chalcogenide glasses have been the subject of the systematic studies for many years because of the changes in physical and chemical properties that occur in these samples after exposure and annealing [1–7], and because of the possibility of fabricating optical elements for applications involving submicron lithography, holography, optical memories, and imaging.

Recently Messaddeq et al. [8] reported photoexpansion associated with photobleaching in GaGeS glasses. Photobleaching is a photoinduced blue shift of the optical absorption edge, and is accompanied by a decrease in the refractive index in the transparent spectral range below the absorption edge. Photoexpansion is an increase in the volume of a photodarkened (or photobleached, in our case) chalcogenide glass.

In the present work we use the photoexpansion effect to holographically record diffraction gratings on bulk GaGeS glass. The fractional expansion $\Delta V/V$ measured is about 5% in bulk glass and diffraction efficiencies up to 30% are obtained. However, the investigation of the effects of the topography surface on the formation of the periodical interference structure has not yet been widely mentioned.

* Corresponding author.

Recently, atomic force microscopy (AFM) has been extensively used to investigate the interaction of laser beams with surfaces of different materials with nanometer spatial resolution [9–12]. The AFM images of the gratings show a relief grating under the surface of the glass. The aim of this paper is to present the results of an AFM investigation on the influence of the roughness of the GaGeS glass surface on the diffraction efficiency of the photowritten Bragg grating.

2. Experimental

Glass samples were prepared by melting high purity starting elements (Ga, Ge, and S) in a special quartz ampoule evacuated up to 10^{-3} Pa. All procedures including synthesis, distillation and glass production were carried out in a closed system. After melting at 900°C for 6 h the ampoule was removed, quenched in water and annealed at the glass transition temperature, T_g, near 400°C. Glass rods about 60 mm in length and 10 mm in diameter were removed after cutting the quartz ampoule. Pieces of around 2 mm in thickness were cut and polished. Two kinds of polishing were conducted on the glass surface: (i) polishing by a commercial polishing pad during 30 min and (ii) polishing the sample by a pad charged with polishing particles (CeO_2, mean diameter 0.5 μm).

Transmission holographic gratings with period of $\Lambda = 5\,\mu m$ were recorded by two symmetrically incident Ar^+ laser beams of equal intensity. The recording wavelength λ_1 was 351 nm. The probing of the gratings during the record was done with a He–Ne laser ($\lambda_2 = 633$ nm). The average intensity of the beam I_0 was 5 W/cm^2. The He–Ne laser beam did not cause any observable change in the optical property of the glass because of its high transparency at 633 nm.

3. Results and discussion

3.1. Auto correlation function (ACF)

AFM was used to characterize the topography of the glass surfaces on which gratings were photowritten. Fig. 1 shows the image of a grating recorded on a glass surface polished by commercial polishing pad (Fig. 1a) and polished by a polishing pad charge with CeO_2 particles (Fig. 1b). These images were obtained in the contact-topography-mode with the use of a standard head. Fig. 1a shows the superposition of an "imprinted" grating over the topography of the glass.

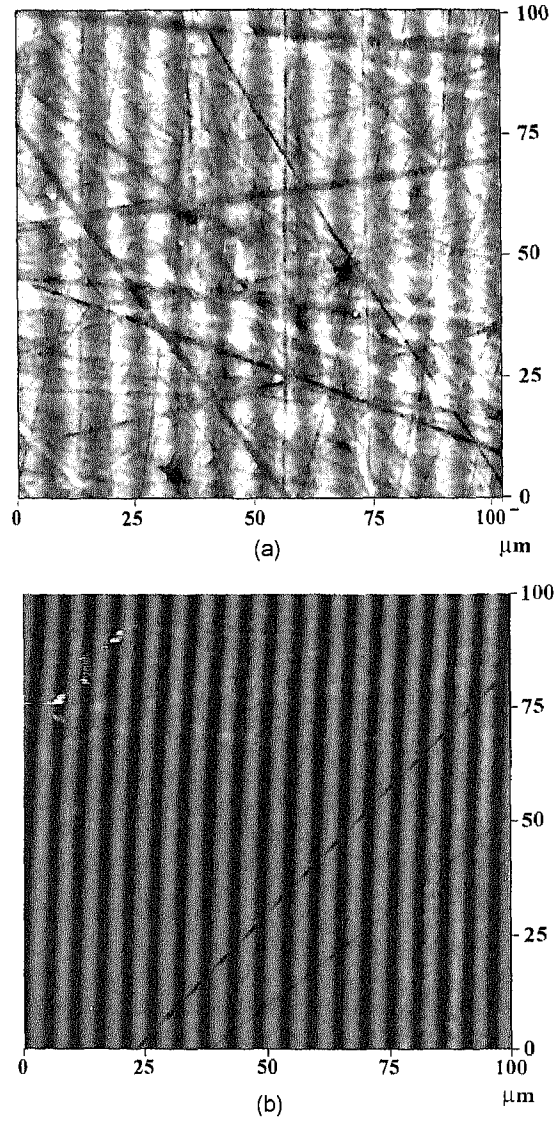

Fig. 1. SFM-image of the surface of the holographic grating in the topography-mode using a standard head. (a) Glass surface polished by commercial polishing pad and (b) polished by a polishing pad charge with CeO_2 particles. Both images show a surface consisting of trenches and grooves, on which a sinusoidal grating has been "imprinted".

Fig. 2 shows the comparison of the diffraction efficiency of the same sample as in Fig. 1. The kinetics

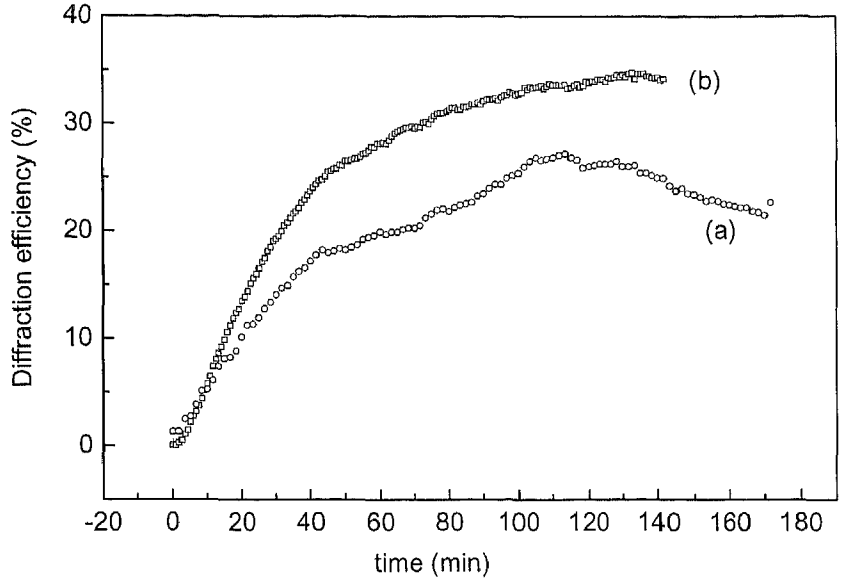

Fig. 2. Diffraction efficiency dependence on time for the sample. (a) Polished by commercial polishing pad and (b) polished by a polishing pad charge with CeO_2 particles.

was probed with a cw He–Ne laser at 633 nm. It is evident from the curves that gratings recorded on the glass surface polished with CeO_2 reached the largest value on diffraction efficiency. The 2D ACF of Fig. 1a given in Fig. 3 shows clearly the auto-correlation-signal of the grating as vertical light bars. Because of the correlation that deteriorates in Fig. 1a, the closer the grating segments are to the margins, the brightness of the bars decreases.

The detailed behaviour of the correlation-function is given in Fig. 4 by showing two profiles, which were produced by a horizontal (upper profile) and a vertical cut (lower profile) through the centre of the 2D ACF. The upper profile in Fig. 4 shows clearly the deterioration of the correlation due to the basic structure of the surface (drop off between the central peak and the following peak) as well as to the likely slightly varying distance of the grating segments in the image (continuous drop off of the peaks towards the margin). The intended constructive interference of the light waves at their reflection at the grating requires, however, the highest and most extended correlations possible, so that the basic structure of the coating as well as the variations of the grating constants reduce the

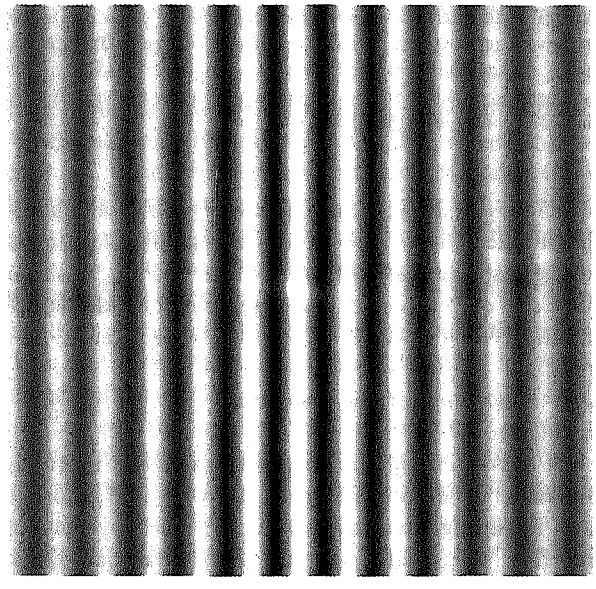

Fig. 3. 2D ACF of Fig. 1a. The peak in the centre of the ACF is caused by the "basic roughness" of the surface of the object, i.e., by the trenches and grooves visible in Fig. 1a. The line type correlation-figure produced by the grating decreases in brightness because of a slight variation of the periodicity of the grating-image from the centre to the margins.

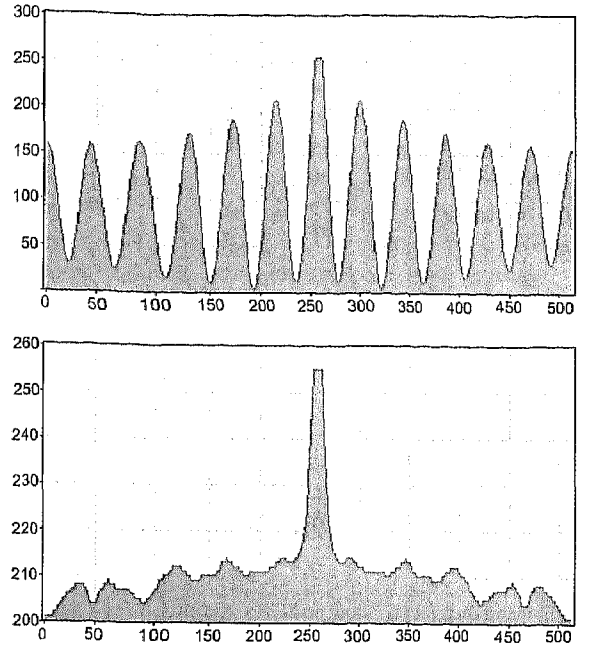

Fig. 4. Horizontal (above) and vertical cut (below) through the centre of the 2D ACF in Fig. 3. The upper profile shows clearly (except for the central peak) an approximated exponential drop of the correlation. The fact that in the upper and lower profile, the central peak clearly overtowers the neighbouring peaks due to the relatively pronounced "basical roughness" of the surface. Apart from the central peak, the peaks in the lower profile are of stochastical nature. Remark: the greyscales mapped onto the y-axis in both profiles are different.

efficiency of the grating. The lower profile, which has been taken in the direction of the grating segments, only grasps the basic structure of the coating. It shows that the correlation of the basic structure drops off relatively fast towards an almost constant level.

3.2. Separation of the structures

A separation of the image-information regarding the basic structure of the glass (trenches and grooves) and regarding the grating was performed by Fourier filtering. This made an artefact free separation of the grating (Fig. 6) from the basic structure (Fig. 5) possible in spite of the overlap of the spatial frequency domains. A proof for the completely artefact free separation of both structures is given in Fig. 7 using the 2D ACF of Fig. 5 (Fig. 7a) and Fig. 6 (Fig. 7b): the ACF in Fig. 7a does not possess a periodical

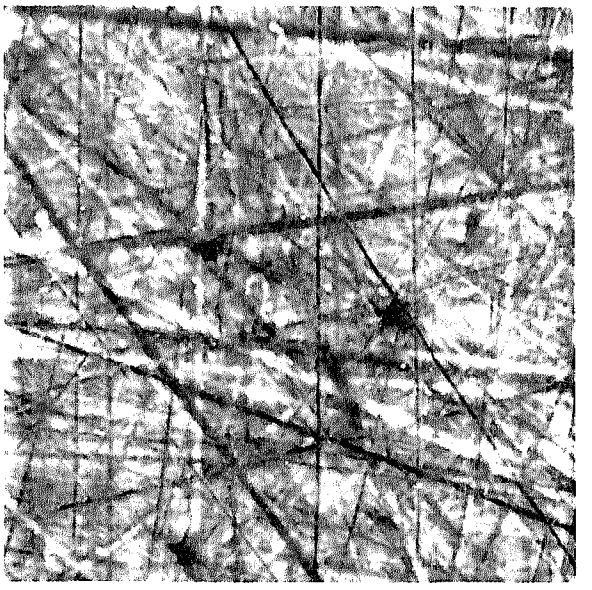

Fig. 5. Image of the "basic texture" of the surface (elimination of the holographic line grating) by Fourier filtering Fig. 1a (elimination of the two reflexes in Fig. 3 and inverse FFT).

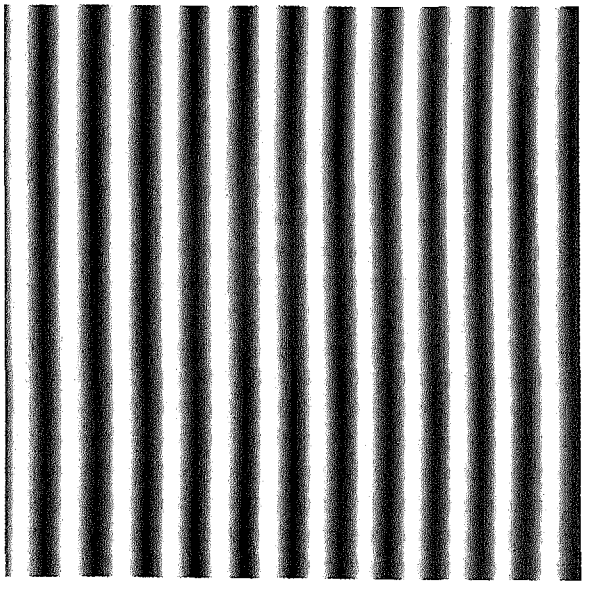

Fig. 6. Image of the holographic grating (elimination of the "basic texture") achieved by Fourier filtering Fig. 1a (selection of the two reflexes in Fig. 3 and inverse FFT).

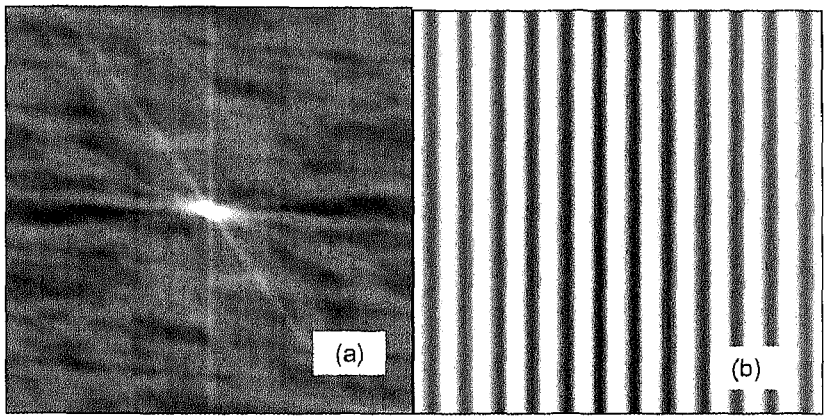

Fig. 7. 2D ACFs of the images of the "basic texture" (a, ACF of Fig. 5) and the grating (b, ACF of Fig. 6). The ACF in (a) proves that all periodical shares of the grating have been eliminated in the image "basic textures" (Fig. 6). The ACF in (b), on the other hand, shows that all information of "basic texture" has been eliminated from the image of the holographic grating (Fig. 6) (peak in the centre of (b) is missing).

auto-correlation-signal and the ACF in Fig. 7b does not have a rotationally symmetric peak in the centre.

Unfortunately, the image processing software used during Fourier filtering stretches the greyscale distribution of the images in an uncontrollable way, so that the determination of the roughness of the separated structures based on Figs. 5 and 6 is not possible. Section 3.3 is concerned with an explanation of a different method by which the surface was analysed.

3.3. Determination of roughness and correlation-lengths

To determine the roughness and correlation-lengths of selected spatial frequency domains, MathCad-programs have been written and applied to the SFM (scanning force microscope)-image of the surface of the holographic grating in Fig. 1a. First, the anisotropy of the roughness for the total spatial frequency spectrum shall be ascertained. Therefore, when we calculate the RMS-roughness

$$\sigma = \sqrt{\frac{\sum_{i=1}^{n}(z_i - z_m)^2}{n-1}}$$

with the heights z_i of the n points of the scanned surface and the arithmetic mean value of these heights

$$z_m = \frac{1}{n}\sum_{i-1}^{n} z_i,$$

we get the roughness independent of the scanning $\sigma = 55.5$ nm (at 50 μm basic length). Only if the above formula is applied to each scanline individually, i.e., if z_m represents the mean value of a scanline and the total roughness is determined through averaging over all N-line-roughness through:

$$\sigma_{tot} = \frac{1}{N}\sum \sigma,$$

then the anisotropy of the roughness can be measured. When scanning Fig. 1a horizontally, we get $\sigma_{tot} = 55.1$ nm, which is identical to the above value (disregarding a statistical error). When scanning vertically, the grating structure is not seen and the result is $\sigma_{tot} = 36.6$ nm. The proportion σ_{tot} (horizontal)/σ_{tot} (vertical) = 1.51 is relatively small, i.e., the grating does not increase the total roughness considerably. This fact could be a source for a possibly low efficiency of the grating.

The spectral roughness was determined using a MathCad-program, which calculates the power functions for the individual line profiles of the SFM-image in Fig. 1a, uses these to determine the average of the power function over all lines, and from these filters out a specific spectral domain to determine the roughness of the corresponding spatial frequency spectrum. In Fig. 8 the power-spectrum gained by horizontally scanning Fig. 1a, is shown on a double-logarithmic scale with the spatial wavelength domains A, B and C used for evaluation. The spectral roughness measured

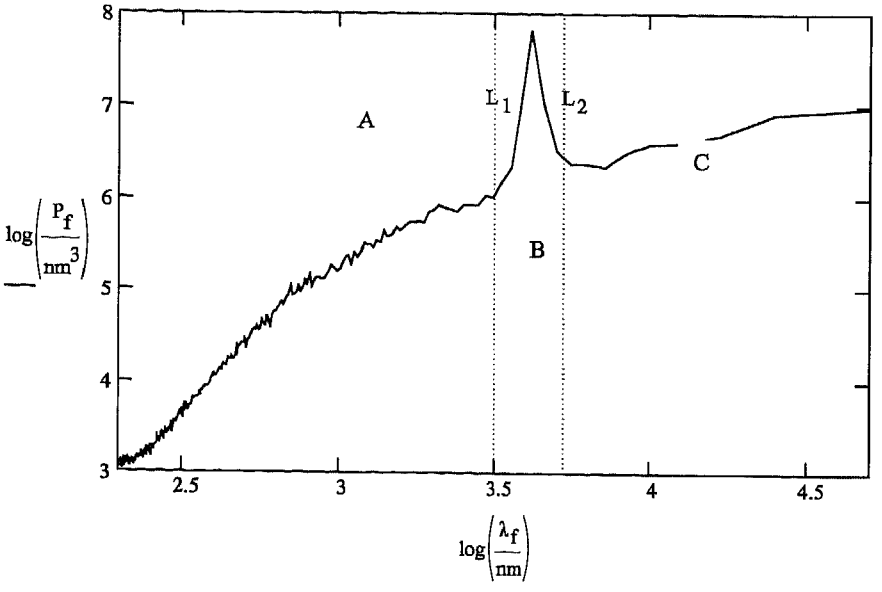

Fig. 8. 1D power-spectrum of Fig. 1a taken in horizontal direction. The power funtion P is reproduced on a double-logarithmic scale as a function of the spatial wavelength λ. The peak, which appears between the limits L_1 and L_2, is caused by the grating. The corresponding spectral RMS-roughness are determined for each of the spatial wavelength domains A, B and C.

for the individual spatial wavelength domains are given in Table 1.

The spectral domain B encompasses the grating, which is clearly visible, because of the peak caused by the grating. The resulting RMS-roughness of the "ideal" grating is with its 43.5 nm (in reference to 50 μm basic length) on the same scale as the RMS-roughness of the basic structure with 34.3 nm (domain A + C). The roughness of the basic structure (in reference to the grasped 50 μm basic length) consists in almost equal parts of a high frequency (A) and a low frequency part (C).

Table 1
The spectral roughness measured for the individual spatial wavelength domains

Spatial wavelength domains	Spatial wavelength attributed to the domains (nm)	Spectral roughness (m) (basic length: 50 μm)
A + B + C	200–50 000	55.3
B	3200–5400	43.5
A + C	200–3200, 5400–50 000	34.3
A	200–3200	21.1
C	5400–50 000	28.2

If the spectral composition of the light, that should be scattered at the grating, is known, then the above spatial wavelength domains A and C can be matched to the spectrum of the light and may result in a lower influence of the basic structure. Under the assumption of an ideal sinusoidal grating, an average variation of the height of the grating $\sqrt{2}\sigma = 61.5$ nm results from the determined spectral roughness of the grating of 43.5 nm.

Another MathCad-program was written to determine the correlation-length of the total structure as well as the correlation-length of the grating. Here the correlation-length for the grating is determined from the drop off of the correlation-maxima. Figs. 9 and 10 show the ACFs of Fig. 1a taken in horizontal direction considering the spatial wavelength domains A + B + C (basic structure + grating) or B (grating). Fig. 9 shows that the "high frequency" roughness (spatial wavelength domain A) of the basic structure immediately reduces the correlation of the grating to approximately 60% (given by the coordinates of the approximation-function for the maxima Yapp), i.e., actually already for $x = 0$. The approximation assumes that the maxima of the ACF are damped exponentially. The logarithmic representation of the

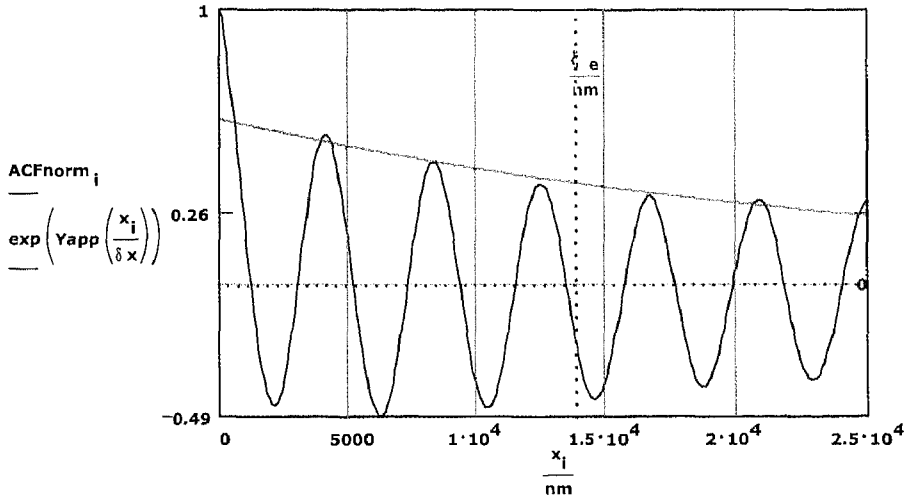

Fig. 9. Standardized ACF_{norm} of Fig. 1a (corresponds to the right half of the upper diagram in Fig. 4) and approximation-function Yapp of the layers of the maxima of the ACF to determine the correlation-length of the grating obtained in horizontal direction.

maxima confirms that the maxima can be approximated by an exponential curve, i.e., by a straight line within the logarithmic representation. This straight line is described by Yapp. However, since Yapp is derived on a pixel basis (f) but in the diagram a length basis (x) is used as abscissa, Yapp is given as function of x/dx (where dx is the length of a pixel). Yapp results as

$$\text{Yapp} = -3.56 \times f - 0.51$$

As can be derived from the comparison of the increases of the approximation-functions Yapp in Figs. 9 and 10 as well as from the course of the ACF in Fig. 11 for bigger x, the further drop off of the correlation of the grating results to a major extent from a slight variation of the grating-distances in the image.

Regarding the last conclusion, we remark that the non-linear scanning of the object surface by the SFM

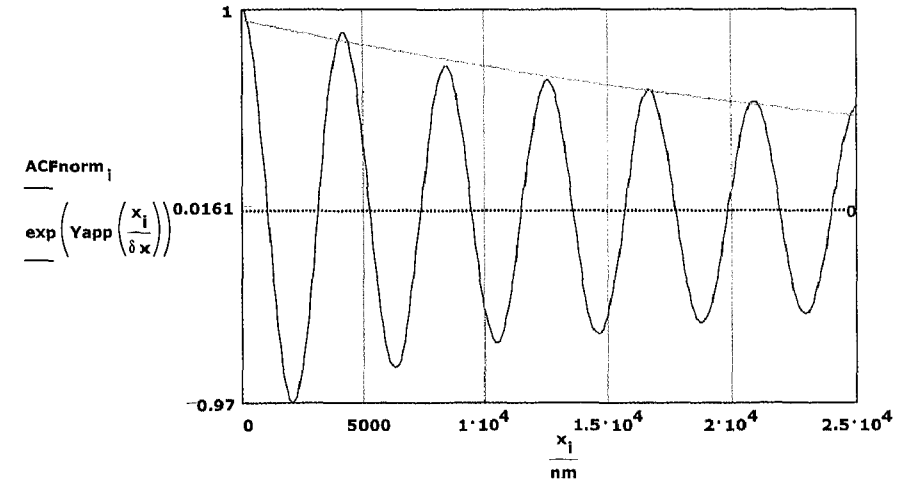

Fig. 10. Standardized ACF_{norm} of Fig. 1a and approximation-function Yapp of the layers of the maxima of the ACF to determine the correlation-length of the grating, obtained in horizontal direction within a predefined window B (3200–5400 nm, see Fig. 8).

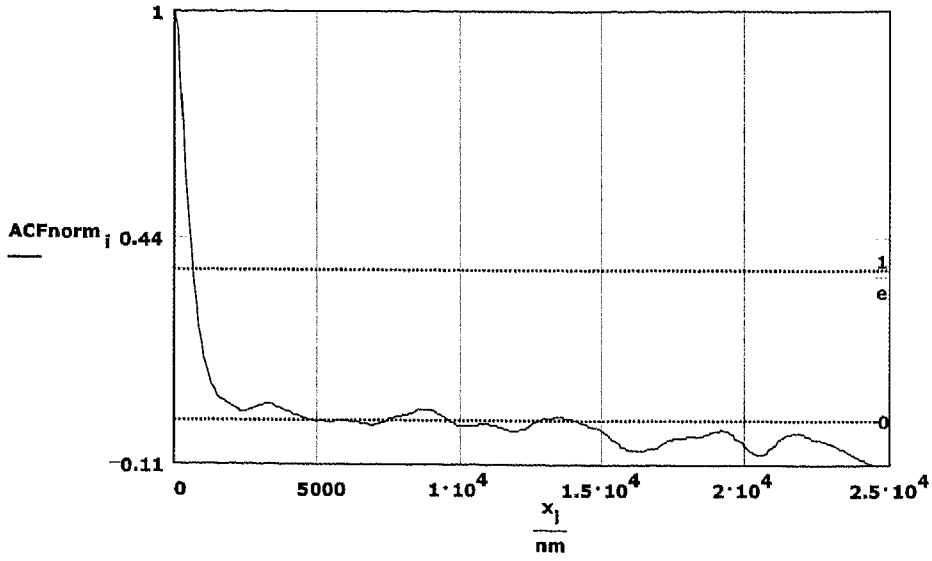

Fig. 11. Standardized ACF_{norm} of Fig. 1a (corresponds to the right half of the lower diagram in Fig. 5), obtained in vertical direction.

Table 2
The correlation-lengths ξ obtained by the above evaluation determined from the drop off of the correlation-maxima

Definition of correlation-length	Horizontal scan, spatial wavelength domain A + B + C (μm)	Horizontal scan, spatial wavelength domain B (μm)	Vertical scan, spatial wavelength domain A + B + C (μm)
ξ of grating re. drop off to 1/e	13.9	33.5	–
ξ of grating re. drop off to 1/10	50.7	79.6	–
ξ of total structure re. drop off to 1/e	0.83	0.79	0.65

may cause the slight variations of the grating-distances in the image. We want to check this assumption by imaging an ideal grating. The correlation-lengths ξ obtained by the above evaluation are put together in Table 2.

4. Conclusion

We have investigated the topography of the photo-written Bragg gratings on a surface of GaGeS glass samples. We confirmed experimentally the effect of the surface polishing in diffraction efficiency of the photowritten gratings. Through Fourier filtering, a separation of both structures, topography and basic was made. As it was not possible to determine the roughness of the separate structure from the image processing software used in Fourier filtering, a separate MathCad-program was written and applied to accomplish this goal.

References

[1] S.R. Elliot, J. Non-Cryst. Solids 81 (1986) 71.
[2] P.J.S. Ewen, A.E. Owen, in: M. Cable, J.M. Parker (Eds.), High Performance Glasses, Blackie, London, 1992, p. 287.
[3] K. Petkov, M. Sachacheva, J. Dikova, J. Non-Cryst. Solids 10 (1988) 37.
[4] I. Konstantinov, B. Mednikarov, M. Sachatchieva, A. Buroff, US Patent 4 499 173 (1985).
[5] K. Petkov, M. Sachatchieva, N. Malinoswski, J. Non-Cryst. Solids 85 (1986) 309.
[6] K. Petkov, G. Kozhuharova, in: Proceedings of the Second East–West Surface Science Workshop, EWSSW'96, Pamporovo, Bulgaria, 1996, p. 284.

[7] H.Y. Lee, H.B. Chung, Jap. J. Appl. Phys. 36 (1997) 2409.
[8] S. Messaddeq, Y. Messaddeq, M. Siu Li, in: Proceedings of the XIIth International Symposium on Non-oxide Glasses and Advanced Materials, Florianópolis, Brazil, 2000, pp. 335–339.
[9] J. Heil, J. Wesner, K. Hilmann, et al., J. Vac. Sci. Technol. A 6 (1988) 401.
[10] A. Bartolome, R. Garsia, L. Vasquez, A.M. Baro, J. Microsc. 152 (1988) 205.
[11] H. Kumagai, M. Ezaki, K. Toyoda, M. Obara, J. Appl. Phys. 73 (1993) 1971.
[12] H. Hiraoka, M. Sendova, Appl. Phys. Lett. 64 (1994) 563.